Materials & Design 257 (2025) 114448

Contents lists available at ScienceDirect

Materials & Design

journal homepage: www.elsevier.com/locate/matdes

High strain deployable interleaved composite flexures

Majed Almuslmani [a,b,*], Matthew Santer [a]

[a] Department of Aeronautics, Imperial College London, London, SW7 2AZ, UK
[b] King Abdulaziz City for Science and Technology, Riyadh 12354, Saudi Arabia

ARTICLE INFO

Keywords:
Controllable stiffness composite materials
Finite element analysis
Viscoelasticity
Deployable structure
High strain composite

ABSTRACT

This study explores the enhancement of high-strain composite flexures by interleaving carbon fiber composite with thermoplastic materials. The flexure significantly loses its stiffness when heated beyond the glass transition temperature of the interleaf material, and it is easily deformed. Upon cooling, the flexure retains its deformed configuration and can recover its original shape upon reheating. Despite the constituent materials lacking inherent shape memory, this shape memory behavior, combined with substantial damping capacity, makes these flexures promising candidates for deployable structures in space applications, where controlled and gentle deployment with minimal risk is essential. A comprehensive finite element modeling and analysis procedure is developed to simulate the behavior of these high-strain composite flexures. The modeling process includes all the phases, stowage, freezing, and deployment, while incorporating the viscoelastic properties of the materials. Experimental tests confirmed the accuracy of the FE model in predicting the behavior of these flexures under different conditions.

1. Introduction

Deployable space mechanisms are crucial systems that enable large structures, like solar panels and sensors, to be folded and stowed within a spacecraft. This reduces the overall volume of the spacecraft, making it possible to fit it inside the limited volume of a launch vehicle fairing. When the spacecraft is in orbit, these mechanisms can deploy the stowed structures to their final operational position. The utilization of high-strain composite (HSC) flexures is a key advancement in spacecraft technology, enabling the efficient stowing and deployment of spacecraft structures [1–5]. HSC flexures are constructed from ultra-thin composite materials, allowing them to be folded to a large curvature, and upon release, deploy and recover their initial shape [6–12].

HSC flexures are an attractive choice for spacecraft design and space missions for deploying structures due to their lightweight materials, ease of manufacturing, reliability, and precise pointing accuracy [13–15]. However, they have limited damping capabilities, which may cause problems during deployment. When strain energy is suddenly released, it can generate shock loads or lead to inconsistent deployment, increasing the risk of failed deployment, particularly when HSC structures are stiffer [16]. For example, solar panels may overshoot their final position and collide with the spacecraft bus structure, which can harm the solar cells on the deployable panel and lead to space mission failure [17]. Despite this, it is essential to design stiffer HSC flexure to provide the necessary support against micro-vibration and thermoelastic effects after deployment.

Research has been conducted to investigate the deployment process of structures made of high-strain composite materials, with the primary goal of preventing shock loads and excessive displacement during deployment. The objective is to obtain a high-stiffness structure while ensuring controlled, damped, and full deployment. One approach to achieve this goal is using carbon fiber-reinforced shape memory polymer materials (SMP) [18]. They remember their original shape and return to it after deforming. In addition, they possess damping capabilities, making them excellent at dissipating mechanical energy and dampening kinetic energy [19–25]. However, these SMP composite hinges may fail under a large stowage curvature because of using stiff SMP, which causes the composite hinge to damage at high strain [26,20,27]. To address this, Composite Technology Development, Inc. (CTD) has created composite material TEMBO® [20], which is made of a thermoset SMP. It is used to develop a composite hinge known as the elastic memory composite (EMC) hinge that has the ability to bend to a large curvature with over 5% strain limit without getting damaged [28]. They have effectively demonstrated the development of space structures like solar panels and antennas using EMC materials [16,20,29]. However, the design and analysis of EMC materials must be carefully considered to

* Corresponding author at: King Abdulaziz City for Science and Technology, Riyadh 12354, Saudi Arabia.
E-mail address: malmuslmani@kacst.gov.sa (M. Almuslmani).

https://doi.org/10.1016/j.matdes.2025.114448
Received 6 May 2025; Received in revised form 6 July 2025; Accepted 22 July 2025

Available online 29 July 2025

prevent damage from elastic micro-buckling beyond its limit. There is still a limited understanding of the nonlinear behavior of micro-buckling in elastic polymer fibers [26,30]. Another technique that can eliminate shock load during deployment is a hybrid hinge [17,31,32]. This technique considers designing a hinge using multiple parts of HSC flexure and shape memory polymer or alloy materials. While the HSC parts provide the required stiffness for deployment, the shape memory materials act as a damper [31,33,17].

Finite element (FE) modeling is well-suited for analyzing and designing deployable hinges and flexures in foldable composite systems [34–37]. Ahmed et al. developed a multiscale FE model to simulate the folding and deployment behavior of origami-inspired dual-matrix composites, incorporating elasticity, plasticity, viscoelasticity, and hyperelasticity [38]. Din et al. proposed an FE modeling approach to predict changes in the electrical resistance of rGO-coated fabric sensors embedded in origami-style composite structures, using the UMATHT subroutine in ABAQUS [39]. In a separate study, Ahmed et al. utilized X-ray micro-computed tomography (XCT) to assess the mechanical properties of ultra-thin composite materials designed for origami-inspired deployable structures. The properties obtained from XCT were subsequently applied in finite element modeling to analyze the folding and deployment of the origami structure [40].

This paper introduces the use of carbon fiber composites with thermoplastic interleaf materials, referred to as Controllable Stiffness Composite Materials (CSCM), to develop high-strain composite flexures. These flexures aim to mitigate risks associated with shock loads and excessive movement during deployment. CSCM offers flexures with shape memory capability and considerable damping, which make them attractive for developing deployable flexures with controlled and smooth deployment. The constituent materials used in CSCM do not inherently have shape memory. However, incorporating a thermoplastic material layer into a carbon fiber composite flexure enables it to exhibit this ability. This distinguishes CSCM from SMP composites, where the shape memory originates from the polymer matrix [41,42]. The term "shape memory" is used here in a general sense to refer to the ability of the CSCM structure to return to its original shape after thermally induced deformation and release, rather than to imply the use of conventional shape-memory alloys or shape-memory polymers.

A similar structural concept to the CSCM structure was developed by Gandhi et al. [43,44]. They created a beam of multiple aluminum layers, and between each two aluminum layers, a layer of polymer was placed and attached to them with adhesive. The beam starts to lose its flexural stiffness upon heating, whilst its damping increases. An initial investigation study of the shape memory of CSCM was carried out by researchers at Imperial College London [45]. Since then, more studies on CSCM structure have been conducted.

Maples et al. [46] examined the storage modulus of carbon fiber composites interleaved with polystyrene at an elevated temperature. They conducted flexural tests using a DMTA machine on various configurations of these composites. The samples were heated from 20 ^{o}C to 120 ^{o}C during the tests, and as the temperature increased, their stiffness decreased. However, when the samples were cooled down to 20 ^{o}C, they fully recovered their initial stiffness. Depending on the layup, the reduction in flexural stiffness at 120 ^{o}C was shown to be up to 98% of the stiffness at 20 ^{o}C. Furthermore, microscopic photos showed relative sliding between the carbon fiber layers under loading at 120 ^{o}C, indicating decoupling between these layers. Zhang et al. [47] explored the influence of the interleaf material viscoelasticity on the load while reshaping a CSCM structure. Their findings indicate that lowering the loading rate reduces the bending load needed for the stowage process because a significant relaxation occurs in the modulus of the interleaf material. Robinson et al. [41] conducted experiments on CSCM specimens with angled cross-sections to demonstrate their shape memory capability. Some specimens were initially shaped into a U-shaped geometry with parallel sides, while others were reshaped into a flat geometry. In both cases, the specimens successfully returned to their original shapes. The specimens were composed of thick composite carbon fiber layers with a high fiber volume fraction. Thus, microscopic images revealed breaks in some CF layers, although the specimens did not exceed a 45^{o} on either side. Also, Maples et al. [48] conducted experiments to investigate the shape memory of a CSCM spring. The findings indicated that it can be easily reshaped with a small load and recovered 99.5% of its original shape when heated. In addition, Murali [49] proposed using a stainless steel layer as a heater positioned between two layers as a heat source for the CSCM structure. This method is considered more efficient and poses a lower risk than attaching a heater to the surface of the CSCM structure using an adhesive, which can separate at very low temperatures due to differences in thermal expansion. However, this approach may reduce the achievable stowage radius with HSC flexure by increasing stiffness and adding mass to the flexure.

Prior research [46,50,45,41,47–49] has focused mainly on examining the main characteristics and mechanical behavior of CSCM structures through experiments, with less attention given to modeling and analysis methods. For instance, Robinson et al. [41] calculate the spring back of a CSCM structure using classical laminate theory. Similarly, Zhang [51] obtained the spring-back of CSCM beams using finite element analysis. However, these studies have not addressed the modeling of recovery and deployment of CSCM structure, nor have they explored the impact of viscoelasticity on the recovery process. Their primary focus was on calculating the spring back after stowage. Besides, the modeling and experiments in these studies have been limited to thick and stiff laminates that cannot withstand high strain without failure, thereby constraining their stowage curvature. A large stowage curvature in CSCM structures introduces geometric and material nonlinearities, making the modeling process more complex. This also leads to high shear strains on the interleaf material, which can cause distortion in the finite element mesh and affect how well the analysis converges. Addressing these issues is crucial for achieving reliable predictions and performance for CSCM structures during deployment and recovery.

To address these issues, this paper proposes a modeling framework that employs the FE method using ABAQUS to simulate and analyze CSCM structures. The emphasis is specifically on the deployment of CSCM flexures designed for space-deployable structures. The study includes experimental validation to evaluate the proposed FE modeling technique in predicting the mechanical behavior of CSCM flexure. It also demonstrates the potential of the CSCM structure as a deployable high-strain composite flexure with damping and shape memory capability. The developed modeling and analysis approach incorporates the viscoelastic behavior of both the carbon fiber composite and interleaved polymer layers, with a focus on their influence during the deployment phases of the CSCM flexure as it returns to its original geometry.

The paper is arranged as follows. In Section 2, the FE modeling and analysis procedure of CSCM flexure is presented. The validation process of the finite element methodology is outlined and examined in Section 3. Thus, the numerical results obtained through implementing the FE procedure are compared with the experimental results, highlighting their correlation. Section 4 includes the conclusion and summary of the paper, where the key findings and insights are summarized, and the implications of the research are discussed. Finally, Appendix A presents the characterization of materials required for the FE simulation, detailing the viscoelastic and elastic properties of both the carbon fiber and interleaf materials. These properties are essential inputs for numerical simulations and experimental validation.

2. CSCM modeling and analysis

Designing a CSCM flexure for use as a deployment mechanism for space applications required developing a reliable modeling and analysis methodology. Thus, it is essential to understand how a CSMC flexure behaves during reshaping and deployment and how it recovers its initial shape.

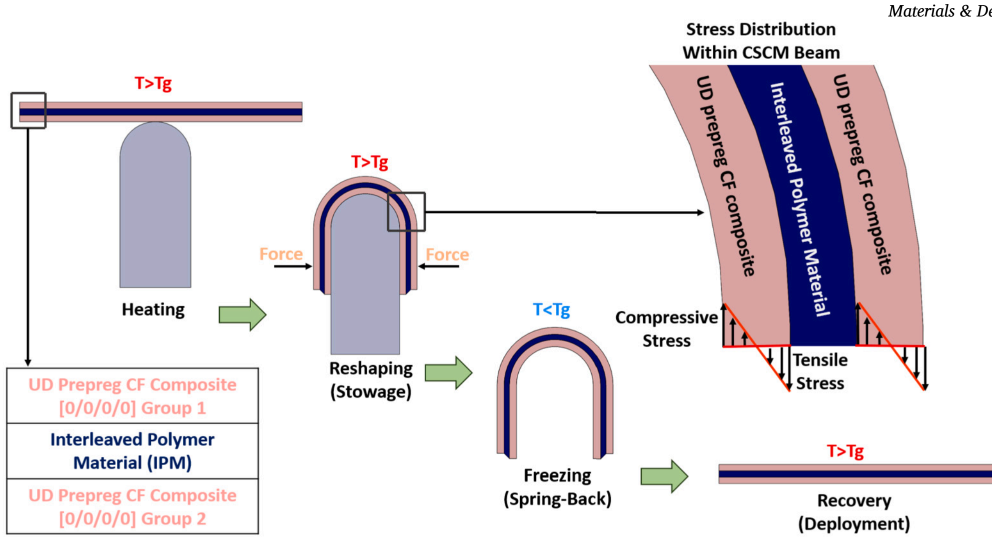

Fig. 1. A CSCM beam, consisting of unidirectional carbon fiber prepreg layers separated by an interleaved polymer layer, undergoes a reshaping and recovery cycle.

Fig. 1 illustrates a beam with two carbon fiber (CF) layers and a layer of thermoplastic material interleaved between them. The stowage process of this CSCM beam begins by heating it at $T > T_g$ of the thermoplastic layer, where T_g is the glass transition temperature. The heating process would cause the interleaf to lose its stiffness, so it becomes less effective in transferring load between the CF layers and effectively causing their mechanical behaviors to decouple. Consequently, the CF layers under loading experience relative displacement to each other, generating high shear strain within the interleaf layer, and the load required for stowage is reduced compared to when $T < T_g$. Furthermore, the stress distribution across each CF layer becomes more uniform, with slight variations due to differences in curvature. This behavior, as displayed in Fig. 1, highlights the existence of decoupling between the two layers, with stress values ranging from maximum tensile to maximum compressive.

Once the CSCM beam is in its stowed configuration, it is cooled below the T_g of the interleaf thermoplastic layer. The cooling process causes phase changes in the thermoplastic from a rubbery to a glassy phase, which decreases the mobility of the molecular chains and locks in its deformation. Hence, the thermoplastic layer will lock the beam in the stowage configuration and counteract the strain energy stored within the CF layers, which would try to retrieve the initial form of the beam. However, spring-back can exist based on the amount of strain energy within the CF layers and how the thermoplastic interleaf material is stiff after the cooling process.

If the CSCM beam is reheated again at a temperature above T_g of the interleaf material, the shape memory effect will be activated. The interleaf material loses its stiffness, allowing the CSCM beam to gradually return to its original geometry, driven by the strain energy stored within the CF layers.

2.1. Finite element modeling of a flat CSCM flexure

The finite element procedure for CSCM flexure presented here can be generally applied. However, to describe and validate the FE procedure, a specific CSCM structure is focused on: a flat beam with a rectangular cross-section. By utilizing this particular structure, the presentation of the FE procedure is facilitated, its effectiveness experimentally validated, and the potential of using the CSCM flat structure for space deployment applications is demonstrated. The CSCM flexure under examination has multiple CF layers separated by thermoplastic layers.

The CSCM flexure has three phases: stowage, freezing, and deployment, and they are modeled and analyzed using the FE software ABAQUS 2018. Fig. 2 shows the complete simulation process schematically. Viscoelasticity of the thermoplastic interleaf impacts the CSCM flexure. For example, during the stowage phase, the relaxation of the interleaf modulus as its temperature increases significantly reduces the total stiffness of the CSCM flexure. During the deployment, the interleaf viscoelasticity would slow the CSCM flexure. Also, the viscoelasticity of the CF layers might affect the precision of regaining the initial flat configuration. Accordingly, it is essential to consider the viscoelasticity of the constituent materials when analyzing CSCM flexure.

2.1.1. Flat-flexure stowage phase modeling

The CSCM carbon fiber groups are modeled using the element (S4R), a shell element with four nodes and reduced integration. Additionally, each lamina within a CF layer includes three integration points across its thickness. The interleaf material is modeled using the linear solid element (C3D8), which has eight nodes. Each interleaf layer is meshed with six elements through the thickness to capture the high strain within them effectively, and full integration is applied to prevent the hourglass phenomenon in the elements. The mesh tie constraint technique *TIE is utilized to connect the shell elements with solid elements. This technique assumes perfect bonding and high interlaminar shear strength between the carbon fiber and interleaved layers. The face size of the interleaved solid element is adjusted to match the size of the carbon fiber layer shell element, ensuring perfect bonding.

To reshape the CSCM flexure into its fully-stowed configuration, a punch and a die with two rigid structures are utilized, as illustrated in Fig. 3a. The punch and die are meshed with rigid elements (R3D4). The rigid components of the die are positioned 30 mm apart at the bottom edges to ensure that, when fully stowed, the flexure conforms to an outer radius of 15 mm. Each rigid structure of the die has a reference point at the center of its bottom edge, as illustrated in Fig. 3b. Fixed boundary conditions are applied to these reference points to fix the die structure during the stowage process. In addition to applying the boundary conditions on the punch, a reference point is used at the center of its curved section, as displayed in Fig. 3b. At this reference point, the punch is constrained except for movement in the Y-direction. To complete the reshaping process, the punch must travel 133 mm in the negative Y-direction. Additionally, to model the friction forces on the surfaces of the CSCM flexure in ABAQUS, a surface-to-surface contact approach is utilized to handle the interaction between the punch, the two rigid structures of the die, and the flat CSCM flexure. The coefficient of friction is 0.01, and it applies to all contact surfaces.

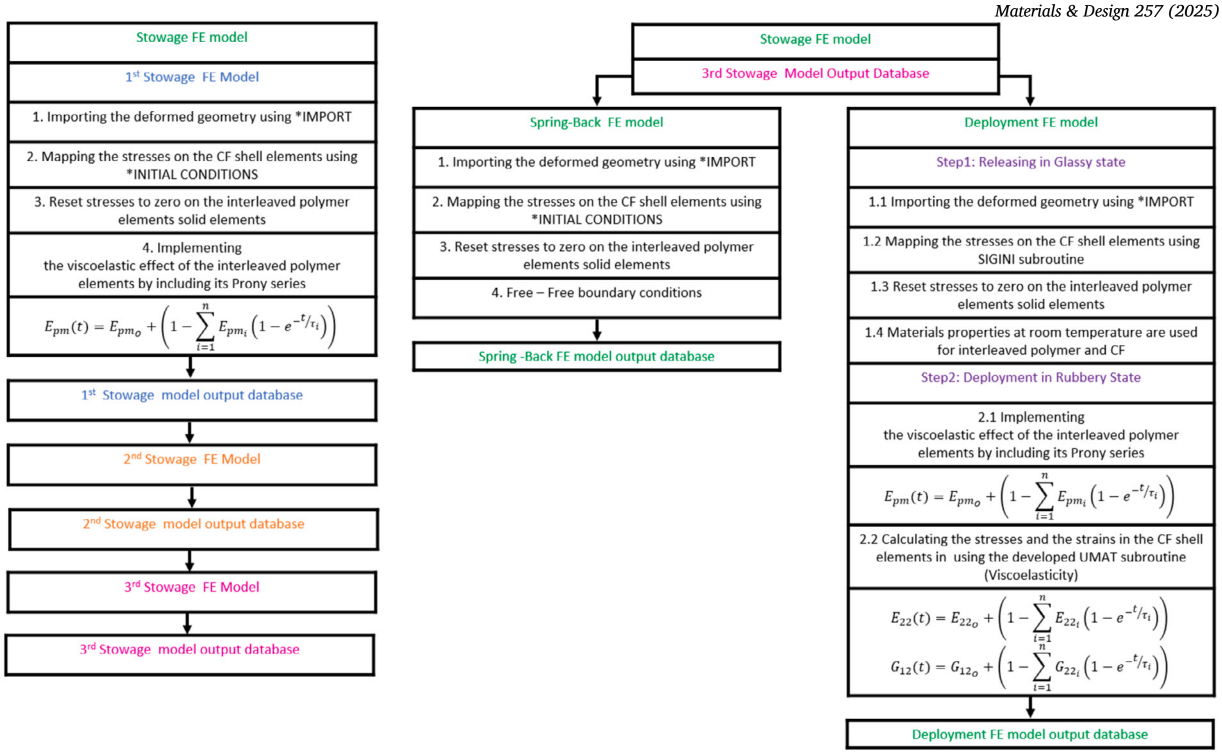

(a) Stowage FE simulation. (b) Spring-back and deployment FE simulations.

Fig. 2. Flow chart of CSCM structure analysis.

The relaxation in the modulus of the interleaf material during the stowage phase is considered in the analysis. In ABAQUS, the relaxation of the interleaf material is included in the analysis using a Prony series. The Prony series representation of the relaxed modulus with time is given as:

$$E_{ipm}(t) = E_{ipm_o}\left(1 - \sum_{i=1}^{n} E_{ipm_i}(1 - e^{-t/\tau_i})\right) \tag{1}$$

where E_{ipm_o} is the instantaneous modulus, τ_i are the relaxation times, and E_{ipm_i} are Prony series coefficients [42].

At high temperatures, the matrix material within the carbon fiber layers undergoes relaxation and lowers the effective modulus of the CF layers. Specifically, there are negligible changes in the modulus along the fiber direction E_{11} but noticeable variations in the modulus perpendicular to the fibers E_{22} and the shear modulus G_{12}. In a symmetric cross-ply layup, these viscoelastic effects of the matrix have an insignificant influence on the bending stiffness D_{11}, which is predominantly influenced by E_{11}. Consequently, the stresses in flexure under bending are relatively insensitive to the matrix relaxation. Therefore, in the analysis of the stowage process, the relaxation of the carbon fiber matrix is neglected, with the stresses in the carbon fiber layers of the CSCM flexure being calculated based on the modulus at room temperature. This assumption could affect the accuracy of spring-back predictions, potentially leading to overestimating the stored strain energy. However, previous research [41,51] has shown that neglecting matrix relaxation during the stowage process has an insignificant effect on the calculated spring-back when using classical laminate theory compared to experimental results.

During stowage, the interleaf layers experience significant shear strain, which becomes more pronounced with the increased stiffness of the carbon fiber layers. This strain causes substantial distortion in the solid elements of the interleaf layers, making it challenging to achieve solution convergence. Additionally, using a high-density mesh for the interleaved polymer layers is computationally expensive and time-consuming, especially when the stowage modeling results are used for subsequent freezing and deployment simulations.

To address these challenges, a technique involving multiple successive finite element simulations is employed. This method breaks down the stowage process into several stages, each simulated with a separate finite element model. This approach helps prevent excessive distortion within the interleaf elements and reduces the computational resources needed for the simulation. This technique requires assuming the elements of the interleaved layers are stress-free as initial conditions in each simulation model.

In each simulation stage, the deformed shape of the previous finite element model is transferred to the new FE model through the *IMPORT command. When dealing with the carbon fibre layers, the stresses from the previous FE model are mapped onto the shell elements of the layers in the new FE model. This process is carried out using the *INITIAL CONDITIONS command, which connects the shell elements in the new FE model with their original geometric shape from the previous FE model.

The stowage simulation is divided into multiple models because the excessive distortion in the solid elements of the interleaf makes it challenging to achieve convergence in the solution. This division requires assuming the interleaf solid elements are stress-free as initial conditions in every finite element model of the stowage. The stress-free assumption in the solid elements that represent the interleaved layers is assumed based on the stress relaxation in polymer materials. When heating a polymer material above its T_g, the polymer chains become mobile, allowing them to move and rearrange freely about each other. This mobility enables the material to adjust its internal structure to dissipate external forces, leading to stress relaxation. However, when the temperature drops below T_g, the mobility of the polymer chains is lost, and the material becomes stiff and locked in a new configuration with residual stresses. Despite this, these residual stresses may be disregarded [52,53,51,49,54].

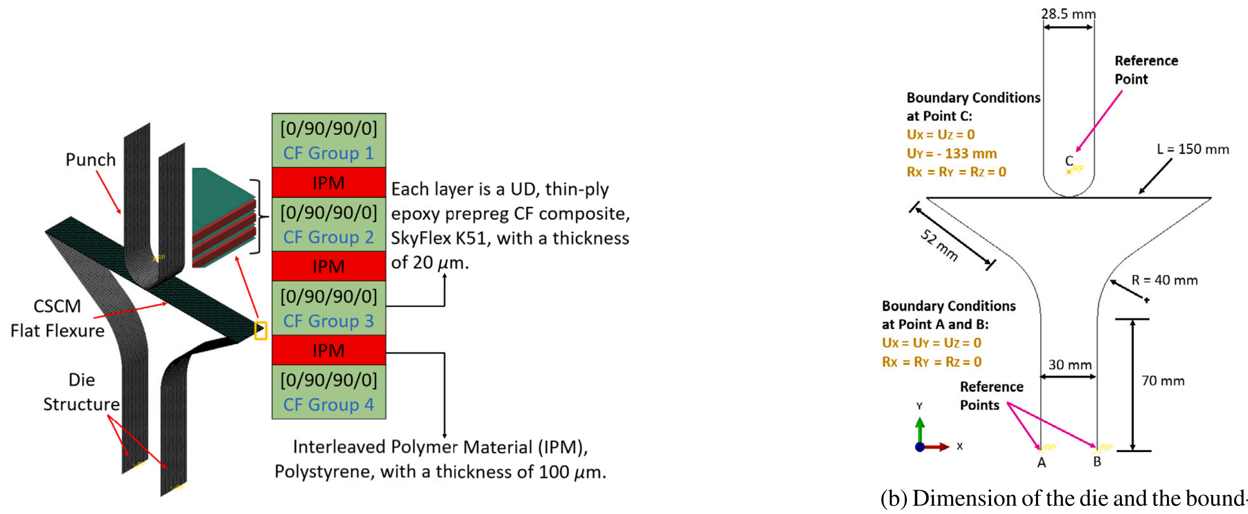

(a) The assembly of the meshed parts in the stowage FE model.

(b) Dimension of the die and the boundary conditions.

Fig. 3. Schematic of the modeling of the CSCM flexure storage process, where the flexure is composed of unidirectional (UD) epoxy-based carbon fiber prepreg layers (SkyFlex K51) separated by interleaved polystyrene layers.

2.1.2. Freezing phase model

The spring-back in the CSCM flexure occurs after it is reshaped into the stowage configuration, and then its temperature drops below the T_g of the interleaf material. If the spring-back is large, it can be harmful as the rebound may result in an unwanted shock load. Additionally, it can cause failure and damage to the interleaved layers, leading to separation between them and the CF layers. How much the CSCM flexure springs back depends on the energy stored in the CF groups during stowage and on the rigidity the interleaved layers attain once cooled. An FE model, namely the freezing FE model, is developed in this section to determine the spring-back amount.

The CSCM flexure is secured between two rigid structures after the stowage process, while its temperature drops to room temperature. As the temperature decreases below the T_g of the interleaf material, it transitions from a rubbery to a glassy phase, and its modulus increases until it is fully recovered at room temperature. Additionally, the molecular chains within the interleaf become significantly less mobile, locking the material into the deformed shape and causing it to maintain the stowage configuration. Moreover, the residual stresses within the interleaf are expected to be minimal. Accordingly, the thermoplastic interleaved layers are considered stress-free after cooling, provided that the flexure remains constrained within the die. This constraint ensures the die counteracts the forces generated by the strain energy stored in the CF groups during stowage. Once the CSCM flexure is taken out from the die, the strain energy in the CF groups drives the flexure toward its original flat shape, but the stiffened interleaf resists this movement. Eventually, the strain energy overcomes the interleaf's stiffness, leading to a spring-back effect.

The amount of spring-back is calculated using the freezing finite element model in ABAQUS. To do this, the *IMPORT command is used to import stowage geometry from the final stowage finite element model into a new model. This command only imports the meshed elements of the stowed geometry without the stresses or strains, and the imported geometry has no connection to the original flat geometry of the flexure. This disconnected geometry is ideal for the polymer interleaf layers because changing the phase from rubbery to glassy creates a new state in the interleaved layer with zero stress. However, the imported geometry must be connected to the original flat geometry for the carbon fibre layers. This implies that the freezing FE model must consider that the carbon fiber layers were flat and have been deformed into the stowage configuration. To achieve this, the *INITIAL CONDITIONS command is used. This command maps the stresses of the shell elements from the final stowage FE model onto the same elements in the freezing FE model. There are no boundary conditions applied in this FE model.

Considering the recovery in modulus due to the cooling to room temperature, the material properties of carbon fiber and interleaf materials at room temperature are used in the analysis. Therefore, only the elastic behavior is considered, while the minimal impact of viscoelastic behavior on long-term spring-back is disregarded. Thus, the modulus of the interleaf is

$$E_{ipm}(t) = E_{els} \tag{2}$$

where E_{els} is the elastic modulus at room temperature after recovery. The nonlinear dynamic implicit analysis technique is employed in this FE model. The modeling process to obtain the spring back in the CSCM flexure is illustrated in Fig. 2.

2.1.3. Flexure deployment phase model

The CSCM flexure undergoes a two-step deployment process. Initially, the flexure is released from its stowed configuration while the interleaved thermoplastic material is in its glassy phase. This release causes one side of the CSCM flexure to spring back while the other side remains fixed due to the applied boundary conditions. Following this, the flexure is fully deployed by heating it to a temperature that exceeds the T_g of the interleaf material. The deployment FE model assumes the flexure reaches the deployment temperature instantaneously.

In the release step, we assume the interleaf material is in the glassy phase, so the modulus at room temperature is used. Additionally, the initial stresses in the interleaved thermoplastic layers are set to zero. However, these initial stresses rise sharply due to the spring-back effect, driven by the strain energy in the CF layers as they attempt to return to their original shape.

In the deployment step, the viscoelasticity of the thermoplastic interleaf is included in the analysis, and its relaxed modulus is calculated using the equation (1). The deployment temperature is assumed to exceed the T_g of the interleaf material, so the viscoelastic properties are determined at the deployment temperature. The FE analysis also includes the viscoelastic behavior of the CF layers, modeled using a UMAT subroutine. This subroutine provides a more accurate representation of the deployment process by capturing both modulus and stress relaxation of the CF layers over time.

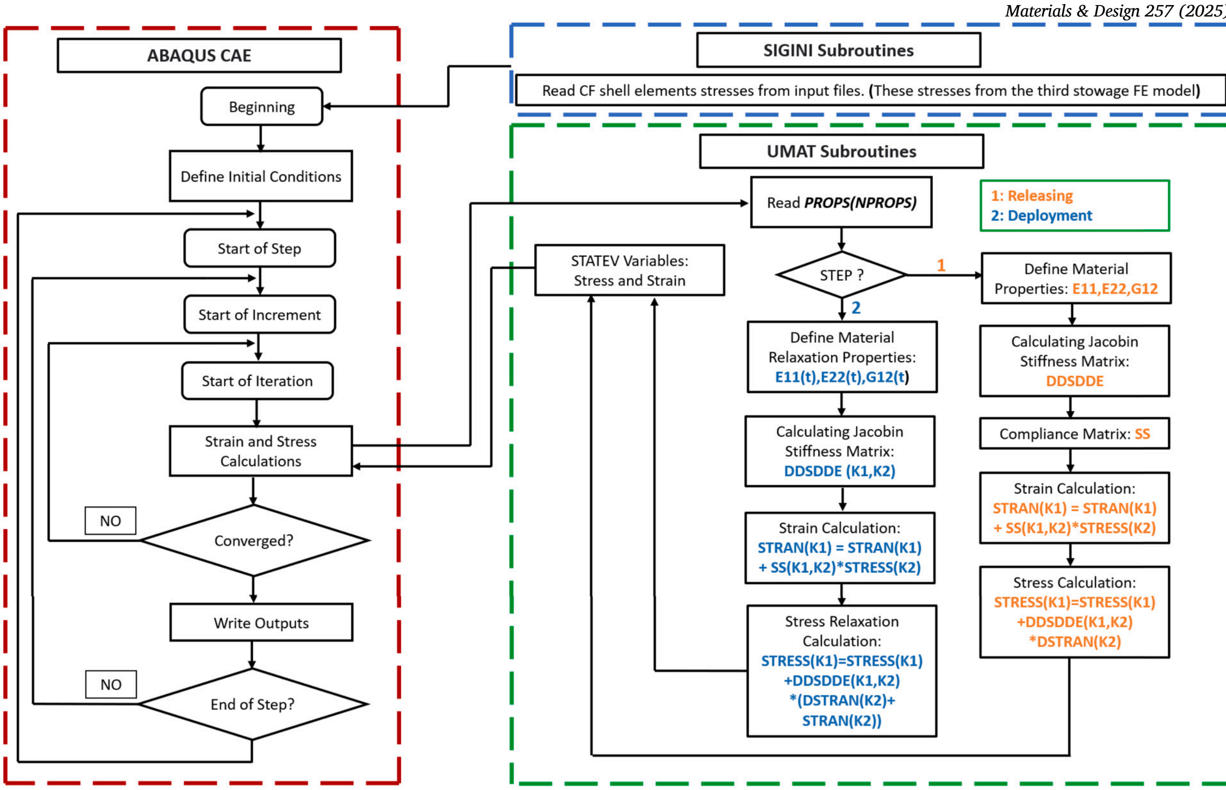

Fig. 4. ABAQUS CAE, UMAT subroutine, and SIGINI subroutine integration flow chart for CSCM flexure stress relaxation.

To develop the deployment FE model, the *IMPORT command is used to transfer the geometry from the final stowage FE model to a new FE model in ABAQUS. Stresses from the shell elements in the stowage geometry are mapped onto the corresponding elements in the deployment model using the SIGINI subroutine, which initializes the stresses in the CF layers. The UMAT subroutine is subsequently utilized to establish the stress–strain behavior of the composite lamina and to compute the corresponding stress values.

$$[\sigma(t)] = [C(t)][\varepsilon(t)] \tag{3}$$

where $[\sigma(t)]$ is the stress, $[C(t)]$ is the stiffness matrix, and $[\varepsilon(t)]$ is the strain.

To simplify the stress-strain relationship for a thin structure, the plane-stress assumption is used here, so σ_3(t), τ_{23}(t), and τ_{13}(t) are set to zero. Thus, the stress-strain relationship in the UMAT subroutine is given as

$$\begin{bmatrix} \sigma_1(t) \\ \sigma_2(t) \\ \tau_{12}(t) \end{bmatrix} = \begin{bmatrix} Q_{11}(t) & Q_{12}(t) & 0 \\ Q_{21}(t) & Q_{22}(t) & 0 \\ 0 & 0 & Q_{66}(t) \end{bmatrix} \begin{bmatrix} \varepsilon_1(t) \\ \varepsilon_2(t) \\ \gamma_{12}(t) \end{bmatrix} \tag{4}$$

where

$$Q_{11}(t) = \frac{E_{11}(t)}{1-\nu_{12}\nu_{21}} \qquad Q_{12}(t) = Q_{21}(t) = \frac{\nu_{12}E_{22}(t)}{1-\nu_{12}\nu_{21}}$$
$$Q_{22}(t) = \frac{E_{22}(t)}{1-\nu_{12}\nu_{21}} \qquad Q_{66}(t) = G_{12}(t) \tag{5}$$

The modulus of elasticity and the shear modulus of the carbon fiber layers are expressed in the UMAT subroutine as Prony series expressions

$$E_{22}(t) = E_{22_o}\left(1 - \sum_{i=1}^{n} E_{22_i}(1 - e^{-t/\tau_i})\right) \tag{6}$$

$$G_{12}(t) = G_{12_o}\left(1 - \sum_{i=1}^{n} G_{22_i}(1 - e^{-t/\tau_i})\right) \tag{7}$$

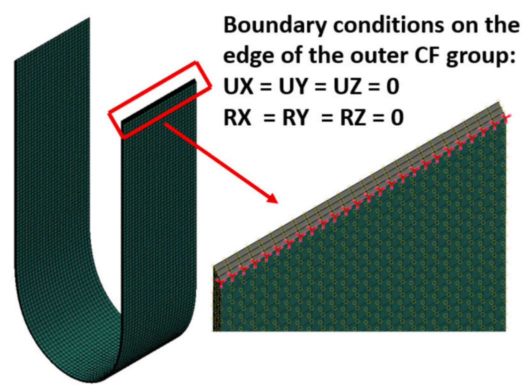

Fig. 5. The outermost CF group has boundary conditions imposed on its edge.

where E_{22_o}, and G_{12_o} are the instantaneous value of the Young modulus and the shear modulus of the carbon fiber layer. In addition, τ_i, E_{22_i}, and G_{12_i} are Prony series constants determined by experiment. Because the relaxation source in the carbon fiber composite comes from the matrix and is not from the fiber, $E_{11}(t)$ is assumed constant with time. The application of the UMAT and SIGINI subroutines in ABAQUS is illustrated in Fig. 4. Additionally, Fig. 2 shows the modeling and analysis process for the deployment of the CSCM flexure.

The simulation of deployment was carried out using nonlinear dynamic implicit analysis. In this simulation, specific boundary conditions were applied to the flexure: one side of the flexure was constrained, and the other remained free. At the constrained end, the edge of the outermost CF group had fixed nodes, creating a rigid support that prevented any rotation or movement at this end. As a result, the other CF groups were able to slide relative to the outer CF group during deployment. The boundary conditions applied during the deployment process are illustrated in Fig. 5.

3. Numerical and experimental results

This section uses a numerical example to evaluate the proposed FE modeling and analysis procedure for CSCM flexure analysis. This numerical example compares the results obtained using the FE procedure with experimental results for validation. Thus, these numerical and experimental studies consider a CSCM flexure with a size of 150×20 mm.

3.1. Fabrication of the flat CSCM flexure

The flat CSCM flexure was fabricated using SkyFlex K51 prepreg, a unidirectional thin-ply epoxy prepreg carbon fiber composite with a nominal ply thickness of 20 μm. The uni-directional pre-preg consists of Mitsubishi Pyrofil TR50S carbon fibers and a K51 resin matrix [55]. The matrix K51 is an epoxy resin system with a curing cycle of 90 min at 125 ^{o}C [56]. This carbon fiber material was selected for its flexibility, making it ideal for constructing compliant composite flexures intended for deployable structures. The materials properties of the prepreg SkyFlex K51 are given in Appendix A.

For the interleaved layers, polystyrene (Styrolution 124N/L) was used. This amorphous thermoplastic material has a glass transition temperature T_g of around 87 ^{o}C and a melting point of 200 ^{o}C [57]. Between the temperature of the melting point and the glass transition, polystyrene exhibits a rubbery state and demonstrates viscoelastic behavior. However, above 160 ^{o}C, the polystyrene begins to show limited viscous flow while still retaining some viscoelastic properties [54]. As the temperature nears the melting range, the material transitions into a fully molten state with increased flow.

The CSCM flexure consists of four carbon fiber laminate groups, each separated by a 100 μm-thick polystyrene interleaved layer. Each laminate group comprises four plies of SkyFlex K51 prepreg arranged in a [0/90/90/0] lay-up configuration. The overall stacking sequence of the flat CSCM flexure is illustrated in Fig. 3a. The fabrication process begins by preparing each carbon fiber laminate group with dimensions of 20 ×150 mm. Using the hand lay-up technique, the SkyFlex K51 prepreg plies are manually stacked in the specified sequence. Three polystyrene sheets, each measuring 20 ×150 mm, are used as interleaved layers and are placed between the carbon fiber groups during layup, as shown in Fig. 3a. The inherent tack of the epoxy prepreg allows the plies and interleaved layers to temporarily adhere to each other during manual assembly, facilitating accurate alignment without the need for external adhesives. Once the lay-up is completed, the assembly is subjected to vacuum pressure at room temperature for 10 minutes to enhance consolidation and improve bonding between the carbon fiber and the interleaved polystyrene layers. The structure is then cured in an autoclave at 125 ^{o}C and 5 bar, resulting in a fully consolidated CSCM flexure of 20×150 mm and average thickness 628 μm.

The reshaping and deployment of the CSCM flexure in this study occur below 160 ^{o}C, eliminating any concerns about the infusion of the interleaved layers into the adjacent carbon fiber layers. Additionally, the carbon fiber matrix of SkyFlex K51 is a thermoset epoxy. Unlike polystyrene, this epoxy does not melt or flow when heated but softens while maintaining its crosslinked structure, ensuring dimensional stability. Previous studies involving similar controllable stiffness composites with interleaved polystyrene have provided Scanning Electron Microscopy (SEM) images supporting this conclusion [45,58,41,51,49].

For example, Maples et al. [46] presented SEM micrographs of a composite laminate composed of HexPly 914C carbon/epoxy prepreg and Styrolution 124N/L interleaved layers, cured at 175 ^{o}C—a temperature higher than that used in our process. Their results show no visible infusion of polystyrene into adjacent carbon fiber layers, even at elevated curing temperatures. This strongly supports the expectation that, under our lower processing temperatures, polymer infusion does not occur, and the interface remains well-defined.

3.2. Stowage phase of a flat CSCM flexure

The stowage process of the CSCM flexure was simulated using three separate finite element models. Each model included a nonlinear quasi-static implicit analysis step that lasted for 120 seconds. This duration was deliberately chosen to ensure that the interleaved polystyrene modulus had enough time to relax and reach a very small value before the punch moved over a long distance. Fig. 17 in the appendix illustrates the relaxation of the PS modulus. The stowage process happens at 120 ^{o}C, and the Prony series coefficients for polystyrene at 120 ^{o}C in Table 3 are utilized to account for the viscoelasticity during the reshaping process. The rigid punch traveled a total distance of 133 mm, equally distributed among the three models. Fig. 6 shows the CSCM flexure before and after the stowage process, and due to the very low modulus of the polystyrene at 120 ^{o}C, the CF groups were able to slide over the interleaved layers, as indicated by comparing the flexure at its ends before and after the reshaping in Fig. 6.

A flat CSCM flexure was manufactured to validate the FE analysis results, and its dimensions, materials, and layup of the CSCM flexure match those in the FE model. Additionally, a rig was designed and manufactured to reshape the flat CSCM flexure into the desired configuration with a 30 mm outer diameter. The rig includes a die and a punch, as displayed in Fig. 7a. The die was placed inside an environmental chamber during the stowage process, which was set on an Instron B 50 kN tensile machine bench to conduct the reshaping process. The reshaping process was conducted at 120 ^{o}C. To achieve precise control over the punch's speed and direction, it was integrated with the tensile machine. This integration ensures high accuracy in the stowed geometry of the CSCM flexure.

The speed of the punch was 5 mm/minute. The stowage of the flat CSCM flexure is illustrated in Fig. 7, comparing the FE analysis with experimental results. The deformed shape of the CSCM flexure closely aligns with the FE analysis results at different punch positions. When the punch moves to reshape the flat CSMC flexure, this causes the angle of the flat flexure to change from 0^{o} when the flexure is entirely flat to 180^{o} when it is in the stowed configuration geometry, where both sides are parallel.

At the end of the stowage process, the FE analysis revealed that all carbon fiber groups exhibit similar stress distributions. For example, similar stresses were observed through the thickness of the elements at the center of the curvature part of the CSCM flexure for each carbon fiber group, as shown in Fig. 8. The results in Fig. 8 show the variation of the stresses through the thickness of each carbon fiber group, with maximum compressive stresses and strains at the top and maximum tensile stresses and strains at the bottom. There is a similarity between the stress and strain patterns of each carbon fiber group, indicating that the mechanical behavior of each group is decoupled, and each carbon fiber group can be treated as a separate unit when designing and optimizing flexure-based structures without affecting the overall performance of the flexure. However, the degree of curvature did have an influence on the stress distribution. Specifically, the carbon fiber group with the smallest curvature experienced the lowest stresses, while the group with the largest curvature experienced the highest stresses.

The moment applied by the CSCM flexure at reference points A and B after completing the stowage process was 19.17 N.mm. This moment, obtained using the FE method, is validated using experimental measurement. Therefore, a custom-designed test rig, depicted in Fig. 9, is used to validate the moment. The rig has two supports, each comprising a metal block connected to a hollow shaft. Strain gauges are attached to the hollow shafts to measure the applied moment when torque is applied to the metal block. The boundary conditions from the FE model were replicated in the experimental setup. Thus, two rigid beams were 3D-printed and attached to the metal blocks. The two beams represent the rigid structures in the FE model. The distance between the beams is set to 30 mm to prevent spring-back in the CSCM flexure. This enables the CSCM flexure to apply forces on the rigid beams, which exerts a mo-

(a) The CSCM flexure edge before deformation

(b) The CSCM flexure edge after deformation

Fig. 6. Reshaping process of the CSCM flexure using the stowage FE model.

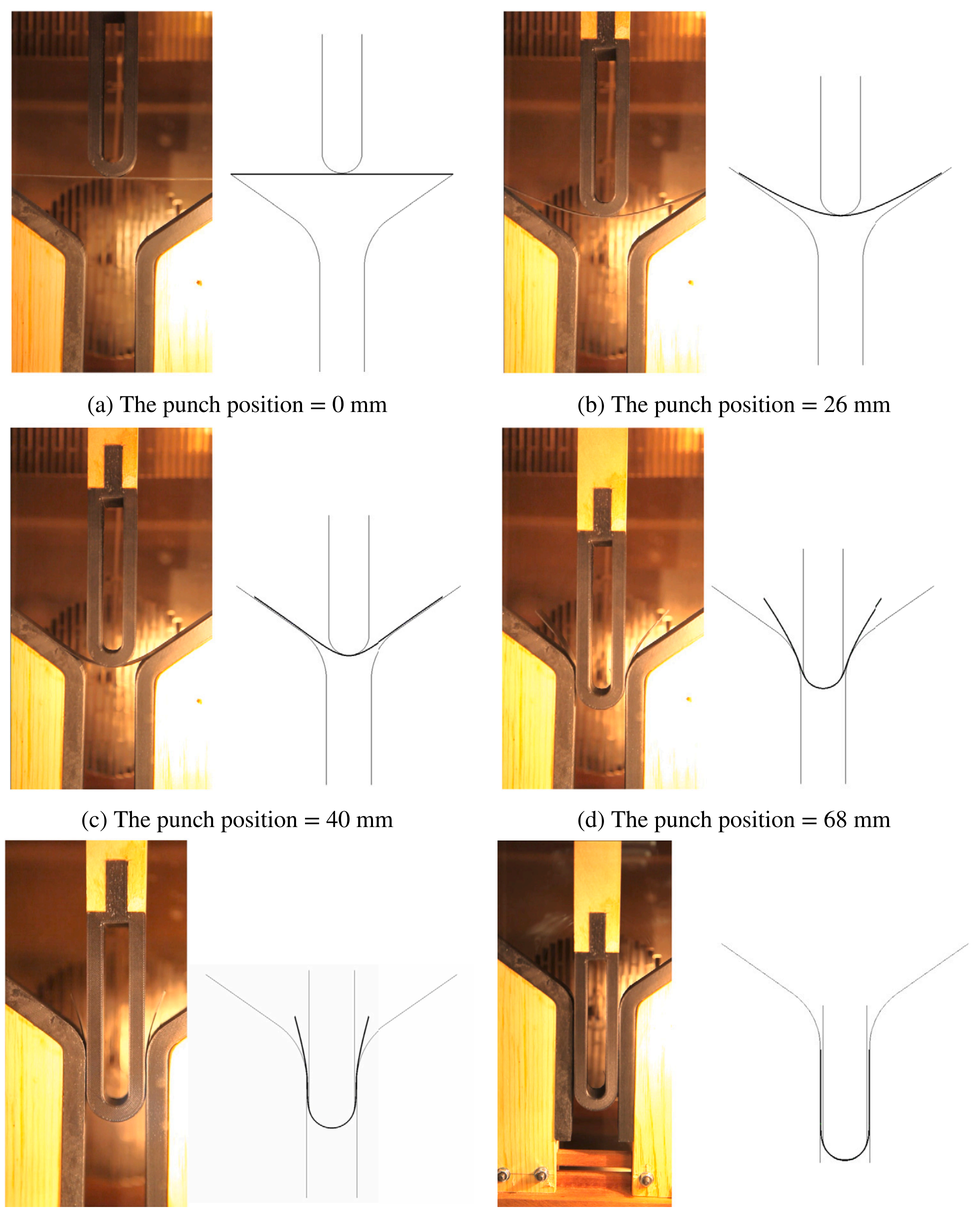

(a) The punch position = 0 mm

(b) The punch position = 26 mm

(c) The punch position = 40 mm

(d) The punch position = 68 mm

(e) The punch position = 92 mm

(f) The punch position = 130 mm

Fig. 7. Experimental and FE analysis results of the CSCM flexure during the stowage phase.

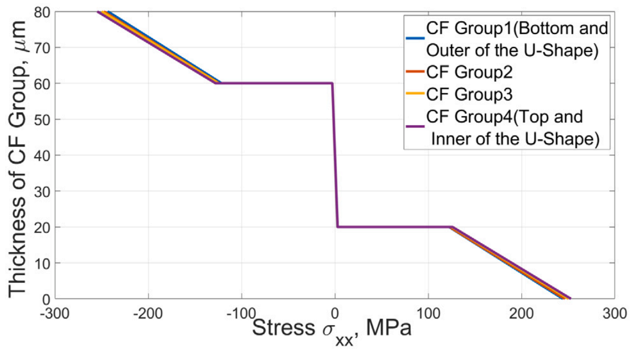

(a) Stress σ_{xx} through the thickness of each carbon fiber group.

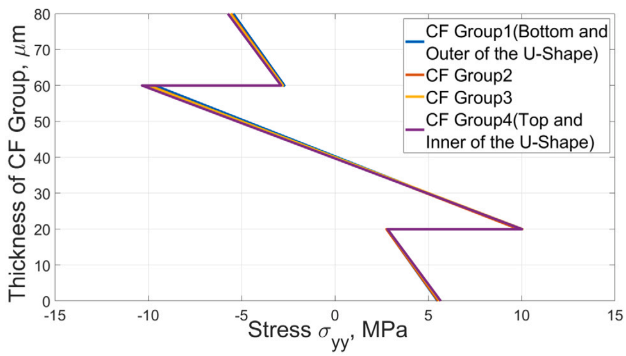

(b) Stress σ_{yy} through the thickness of each carbon fiber group.

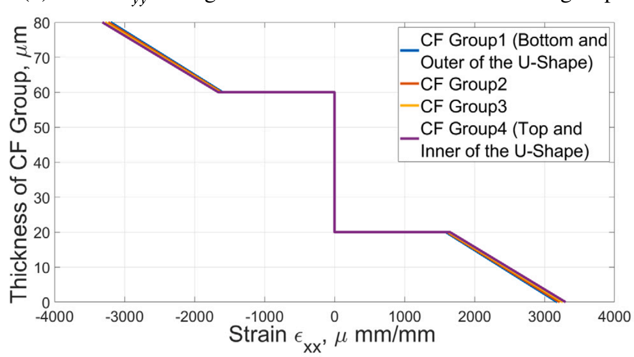

(c) Strain ϵ_{xx} through the thickness of each carbon fiber group.

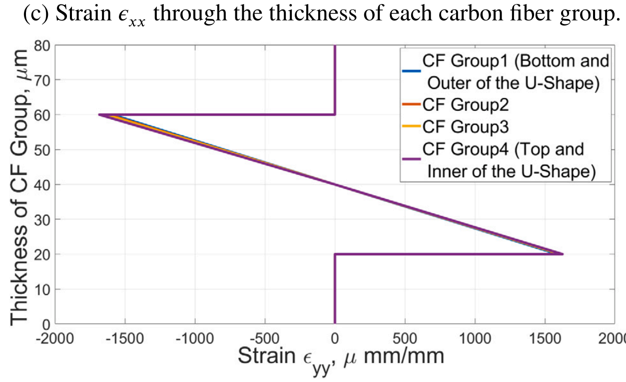

(d) Strain ϵ_{yy} through the thickness of each carbon fiber group.

Fig. 8. Maximum stresses and strains through the thickness of each carbon fiber group.

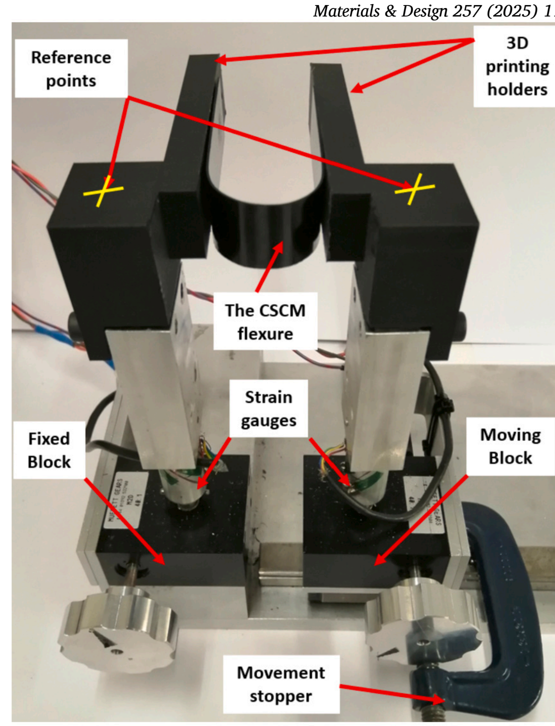

Fig. 9. Measuring the moment of the stowed CSCM flexure.

ment that is measured at the reference points shown in Fig. 9. These reference points correspond to the reference points in the FE model.

Once the CSCM flexure is reshaped, it is firmly clamped between the two rigid beams, and the moment is measured. The moment is found to be 19.195±0.369 N.mm. In the finite element analysis, the moment is 19.17 N.mm. The difference between the experimental measurement and the FE analysis results is only 0.12%, confirming the FE analysis accuracy.

3.3. *Freezing phase of the flat CSCM flexure*

Fig. 10a illustrates the CSCM flexure in its freezing phase. The result was obtained using the FE analysis described in section 2.1.2. The CSCM flexure undergoes a spring-back of 4^o on each side, resulting in an angle of 172^o between the two straight sections. The analysis employed free-free boundary conditions, and the result was obtained by implementing a nonlinear dynamic implicit analysis.

In addition, Fig. 10b displays the fabricated CSCM flexure after being reshaped into the stowage configuration. After the stowage process, the CSCM flexure was left inside the die until its temperature reached room temperature. Once the interleaved polystyrene material had reached the glassy state, the CSCM flexure was taken out of the die. Both sides of the flexure sprang back by 2^o, resulting in an angle of 176^o between the two straight sides. The FE analysis predicted 172^o after the spring-back happened, indicating a 2.3% error between the measured and predicted results as illustrated in Fig. 10b. Also, there was no failure observed in the experimental sample after the spring back.

3.4. *Deployment of the CSCM flexure*

Fig. 11 illustrates the results of CSCM flexure deployment at 140 ^oC using finite element analysis. The CSCM flexure returned to its original flat geometry after 600 seconds. After 60 seconds of deployment, the angle was 56^o. The modulus of the polystyrene material at 140 ^oC is 0.4 MPa, and it significantly reduces over time because of the viscoelasticity. This means that the carbon fiber groups experienced less resistance from the interleaved polystyrene layers as they slid relative to each other during deployment, reducing the required deployment time.

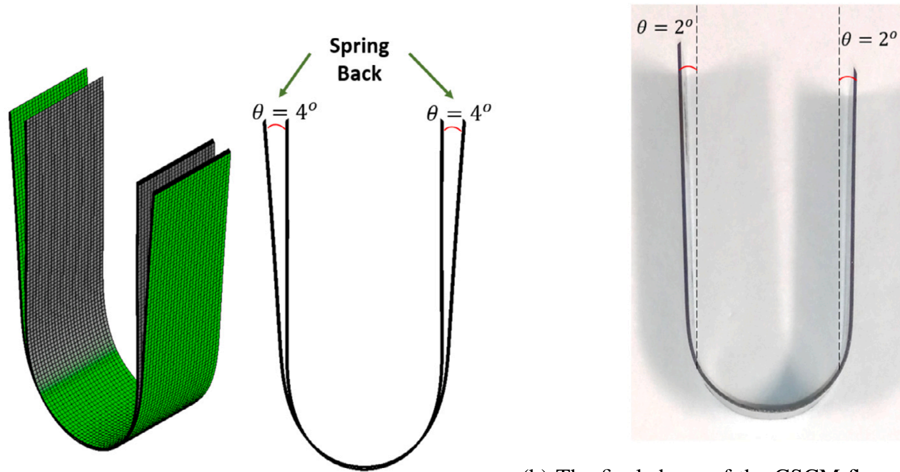

(a) FE analysis results

(b) The final shape of the CSCM flexure after spring back.

Fig. 10. Spring-back of the CSCM flexure: comparison of experimental results with FE analysis.

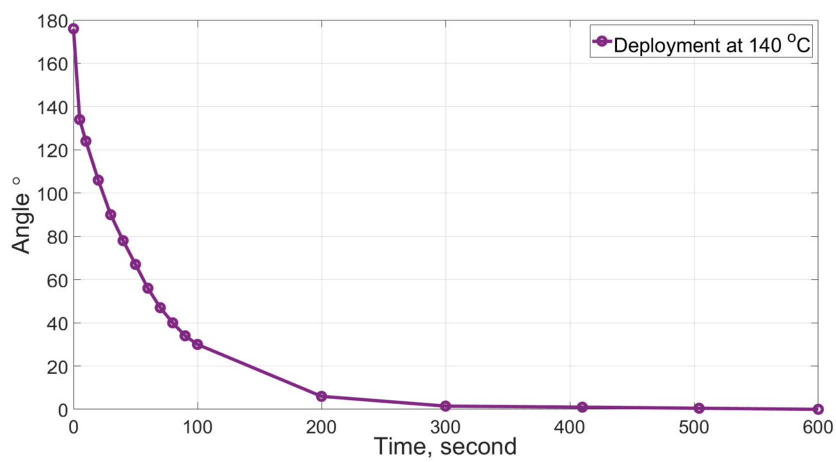

Fig. 11. Deployment and recovery of the flexure at 140^{o}C.

Faster deployment allows for quicker activation of the flexure, which can be critical in mission scenarios where time is a constraint. Fig. 14 illustrates the deployment sequence of the flexure at 140 ^{o}C obtained using the FE analysis.

Deployment and recovery predictions from the FE analysis are validated through experimental investigation of the CSCM flexure. After reshaping, a metal plate is fixed using epoxy adhesive to the outside surface of the flexure at one end. The plat has two holes used to fasten the CSCM flexure to a 3D-printed support structure during deployment using two M2 bolts. This setup ensures that the boundary conditions of the FE model are consistent with the experimental conditions. The deployment takes place inside the environmental chamber at 140 ^{o}C, and the temperature gradually increases until it reaches the deployment temperature.

As the temperature rises, the interleaved polystyrene material softens, which reduces its modulus and allows the CSCM flexure to deploy before it reaches the deployment temperature. To ensure consistency with the FE analysis, the punch was utilized to restrain the CSCM flexure during the heating process, as shown in Fig. 14a, to prevent premature deployment before the desired temperature was reached. This procedure replicates the FE model, where the temperature change happens instantaneously, unlike the gradual increase that occurs inside the environmental chamber. Once the CSCM flexure is heated to the deployment temperature, the punch is removed, and the deployment process starts. To initiate flexure deployment, the punch is pulled upward by activating the tensile testing machine to which the punch is connected. This action removes the punch from the front of the flexure, allowing it to deploy freely. As a result, there is no need to open the door of the environmental chamber to remove the punch, which would cause temperature drops in the flexure.

A digital video camera, the Canon EOS 5D Mark IV, with a 120 frames-per-second capability, is used to capture the deployment process. Five deployment tests were conducted with different CSCM flexures, and Fig. 12 displays the results along with their mean values. Initially, because of the spring-back, the angle between the free and fixed ends of the CSCM flexure is 176^o. The CSCM flexures regained their initial flat shape after 10 minutes. The results of the experiment and FE analysis at 140 ^{o}C are presented in Fig. 13. The experiment results are the mean values of the five deployment tests. Both results are highly consistent, providing confidence in the FE modeling and analysis. Fig. 14 shows the deployment process at 140 ^{o}C of one of the deployment tests. After being exposed to this temperature for 10 minutes, the CSCM flexure returned to its initial flat geometry, indicating the success of the recovery process.

As the temperature increases, the interleaf polystyrene experiences a significant reduction in stiffness. Thus, the CSCM flexure is expected to recover its initial geometry faster when the deployment temperature increases. The carbon fiber layers will face less resistance from the interleaved layers as they become more flexible and soft. To investigate this behavior further, an experiment was conducted to examine the recov-

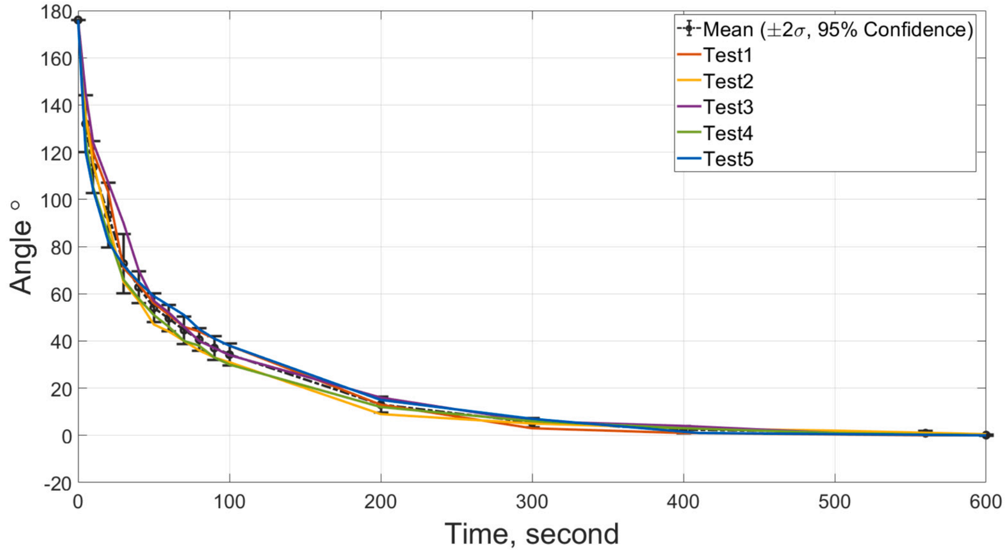

Fig. 12. Experimental deployment tests of the flat CSCM flexure at 140 ^{o}C.

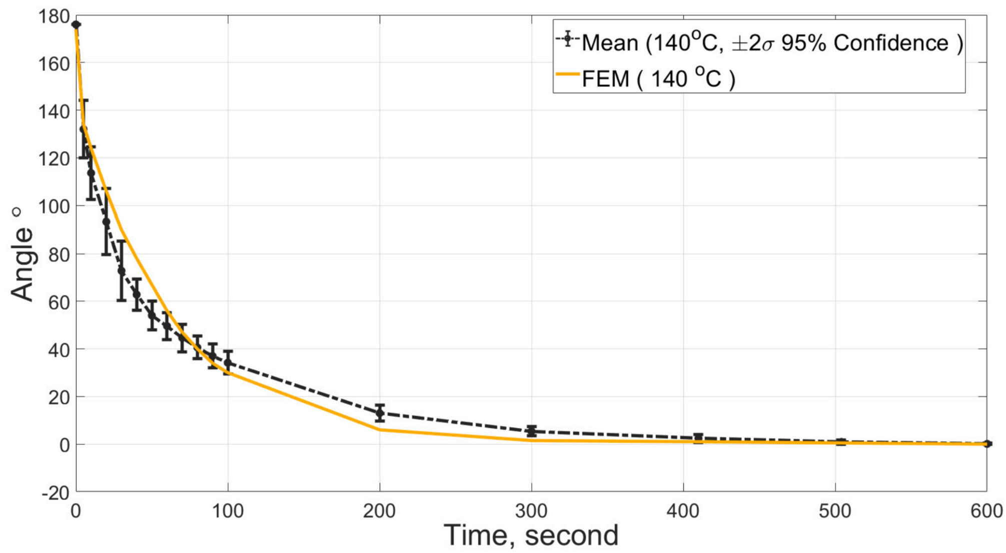

Fig. 13. Deployment results of the flat CSCM flexure at 140 ^{o}C, obtained from both experimental testing and finite element analysis.

ery time at 120 ^{o}C and 160 ^{o}C. Fig. 15 displays the angle of deployment versus time obtained experimentally at 120 ^{o}C, 140 ^{o}C, and 160 ^{o}C. The CSCM flexure could not fully recover its initial flat shape at 120 ^{o}C, resulting in an angle deployment of 54^o after t = 900 seconds. As the deployment temperature increased to 140 ^{o}C, the CSCM flexure recovered its initial shape after 600 seconds, and when the deployment temperature increased to 160 ^{o}C, the recovery time reduced to 35 seconds. The data suggest that the reduction in recovery time is because of the decreased modulus of the interleaved polystyrene layers and their rapid relaxation at higher temperatures, highlighting the impact of their viscoelasticity on the recovery time.

During the deployment tests of the CSCM flexure, heating was applied via an environmental chamber. However, this is not a practical solution in space applications, such as solar panel deployment. Thus, in orbit, thermal activation of the CSCM flexure must be achieved using onboard means. One practical solution is to attach a flexible heater to the surface of the CSCM flexure and provide the required heat for deployment. Such a heater can be adapted to various shapes and is commonly used in space applications. Another way to heat the CSCM flexure is by embedding heater wires within the interleaf materials. In either method, these heaters require electrical power to operate, which can be obtained from the spacecraft's power system. In addition, a temperature sensor and control feedback may be necessary to monitor the heat supplied by the heater and ensure that it provides the required amount of heat for deployment to occur.

4. Conclusion

When interleaving high-strain composite flexure with a thermoplastic material, the flexure would gain shape memory and significant damping, enhancing its performance in space-deployable structures that require smooth and gentle deployment to mitigate risks. In previous research, the shape memory of carbon fiber composites with interleaf material has been investigated through experiments to understand their characteristics and behavior. However, there are limited studies on developing robust modeling and analysis methodologies. In space applications, CSCM flexure may be stowed with large curvature, which requires reliable modeling and analysis techniques to ensure effective performance.

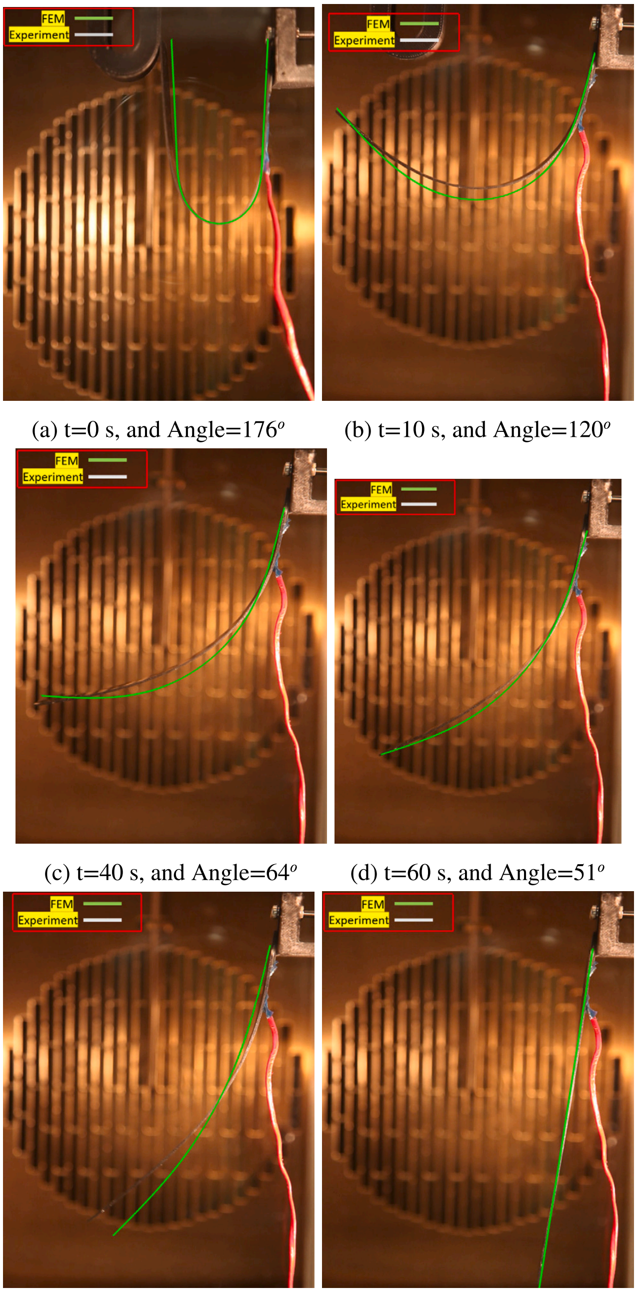

(a) t=0 s, and Angle=176^o (b) t=10 s, and Angle=120^o

(c) t=40 s, and Angle=64^o (d) t=60 s, and Angle=51^o

(e) t=100 s, and Angle=38^o (f) t=600 s, and Angle=0^o

Fig. 14. The CSCM flexure deployment at 140 ^{o}C and the angle corresponding to experimental values.

This paper proposes an FE modeling technique for high-strain composite flexure with thermoplastic interleaf. The CSCM flexure undergoes different stages, including stowage, freezing, and deployment, and its behavior varies with each of these stages. Thus, the FE modeling procedure includes these stages. The FE modeling approach presented here accounts for a temperature-dependent viscoelastic model for both the carbon fiber composite and the interleaf polymer. This enhancement enables more accurate predictions of deployment and recovery behavior in CSCM structures, particularly for thin-ply CSCM flexures subjected to large stowage curvature. Such conditions were not captured in earlier models, which were limited to small-curvature stowage in thick laminates, determining only the spring-back of CSCM structure after the reshaping process. In addition, the FE modeling framework provides a comprehensive procedure to address the challenge of converging results that occur due to high distortion in the interleaved material elements.

During the stowage phase, the interleaf material is under high strain, which causes excessive distortion in the solid elements and leads to difficulties in achieving solution convergence. Thus, the stowage phase modeling was divided into multiple successive FE simulations to eliminate distortion in the interleaf elements and decrease the computational resources required for the simulation. The stowage FE model accounts for the viscoelasticity of the interleaf material, while the viscoelasticity of the carbon fiber layers is excluded, as it has minimal impact on the overall behavior. However, in the deployment FE model, the viscoelasticity of both materials is considered, with the user-material-defined (UMAT) subroutine used to account for the viscoelasticity of the carbon fiber layers.

The FE modeling and analysis methodology was validated through experimental tests. The spring-back observed from the FE analysis was 4^o from each side, while from the experiment, it was 2^o. This shows a 2.3% difference between the FE model and the experiment. Moreover, the deployment results at 140 ^{o}C from the experiment are in consistent with those from the FE analysis, validating the FE approach introduced for the CSCM flexure design and analysis.

The experimental tests have shown that the CSCM flexure deployment and recovery times can be shortened by increasing the deployment temperature. The results have shown that the CSCM flexure, which contains four carbon fiber groups and three interleaved layers, cannot fully recover its original flat configuration within 15 minutes at 120 ^{o}C. However, at 140 ^{o}C, the CSCM flexure was able to return to its flat geometry in just 600 seconds and after 35 seconds when deployed at 160 ^{o}C. These results highlight the influence of the interleaf viscoelasticity on the recovery time.

This study demonstrates the potential use of CSCM structures in spacecraft as deployable flexures with high damping and shape memory capability to achieve controlled and low-impact deployment. The flat CSCM flexure achieved complete deployment with high precision and low shock. This result encourages the investigation of applying CSCM structures to other deployable structures, such as booms and antennas.

Declaration of using AI-powered writing assistant in the writing process

During the preparation of this work, the Grammarly tool was used to check grammar, spelling, punctuation, clarity, and to enhance overall readability. The authors subsequently reviewed and revised the manuscript through multiple drafts and take full responsibility for the final content of the article.

CRediT authorship contribution statement

Majed Almuslmani: Writing – original draft, Visualization, Validation, Software, Methodology, Investigation, Funding acquisition, Formal analysis. **Matthew Santer:** Writing – review & editing, Supervision, Resources, Project administration, Conceptualization.

Declaration of competing interest

The authors declare the following financial interests/personal relationships, which may be considered as potential competing interests:

Majed Almuslmani reports that financial support was provided by King Abdulaziz City for Science and Technology (KACST), Saudi Arabia, as part of his PhD sponsorship through employment.

The other author declares that he has no known competing financial interests or personal relationships that could have appeared to influence the work reported in this paper.

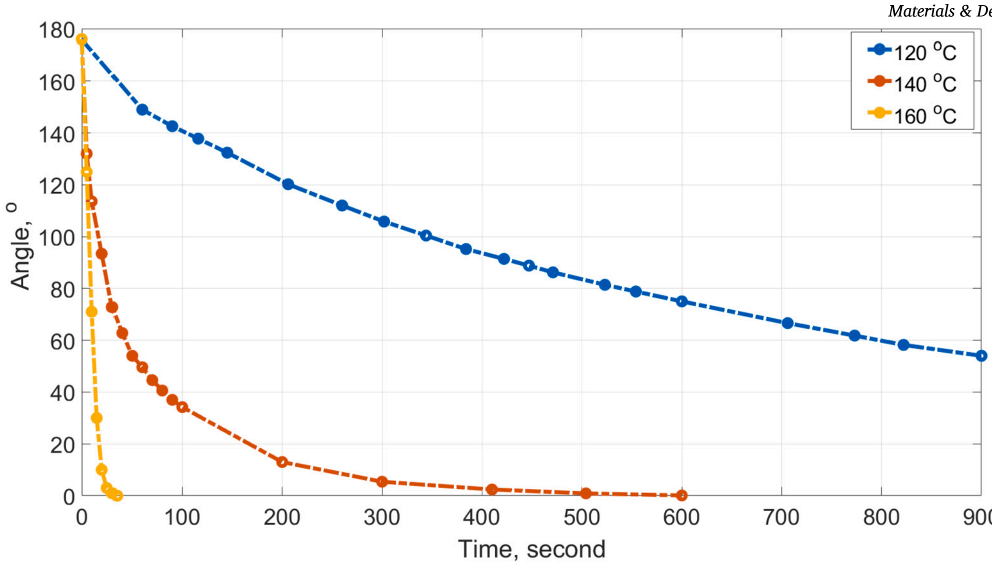

Fig. 15. The effect of deployment temperature on the recovery time of the CSCM flexure.

Acknowledgements

The first author, Majed Almuslmani, would like to express gratitude for the financial support provided by King Abdulaziz City for Science and Technology, Saudi Arabia, as part of his PhD sponsorship through employment.

Appendix A. Material characterization

A UD pre-preg composite material called SkyFlex K51 thin-ply with 20 gsm is used for the CSCM flexure under investigation, and the interleaf material is polystyrene (Styrolution PS 124N/L). To perform an accurate finite element analysis of the CSCM flexure, it is crucial to have a comprehensive understanding of the elastic and viscoelastic properties of these materials [42].

A.1. Thin-ply carbon fiber (SkyFlex K51)

Table 1 gives the elastic properties of the composite material SkyFlex K51. Since the CSMC flexure is subjected to high temperatures during stowage and deployment stages, it is important to evaluate the relaxation behavior of the SkyFlex K51 thin-ply carbon fiber at these temperatures. To achieve this, relaxation tests of the transverse modulus E_{22} were conducted at 140 ^{o}C. The specimens were subjected to tensile strains of 2% for 20 minutes at 140 ^{o}C, and a TA Instruments RSA-G2 Solids Analyzer (UK) was used in tensile mode for this test. The test data, along with the Prony series curves, are illustrated in Fig. 16. The Prony series coefficients at 140 ^{o}C are presented in Table 2.

A.2. Polystyrene PS characterization

The interleaf materials used in this study are polystyrene (PS). The modulus of polystyrene (PS) material at room temperature is 3.2 GPa while the Poisson ratio is 0.35 [41]. The glass transition temperature T_g was found to be 85 ^{o}C [51]. In addition, tensile stress relaxation tests were conducted on Polystyrene (PS) specimens at 120 ^{o}C and 140 ^{o}C using a 5% strain. The specimens were sized at 0.1 × 10 × 15 mm, and the tests were conducted using a TA Instruments RSA-G2 Solids Analyzer (UK) in tensile mode. A constant strain was applied to the specimens at a controlled temperature, and the resulting stress decay over time was recorded. Fig. 17 displays the relaxation results, with the corresponding Prony series coefficients from the relaxation tests provided in Table 3-4.

Table 1
The elastic mechanical properties [59].

Properties (unit)	Values
Tensile modulus, E_{11} (GPa)	76.47
Transverse modulus, E_{22} (GPa)	6.15
Poisson's ratio, ν_{12}	0.28
In-plane shear modulus, G_{12} (GPa)	2.5

Table 2
Prony series relaxation coefficients for the transverse modulus E_{22} at 140 ^oC.

Term	E_{22_i}	Relaxation Time τ_i (s)
1	0.13	1.95
2	0.59	64.00
3	0.01	214.24
4	2.32	75411.37

Table 3
Prony series coefficients to obtain the modulus relaxation of polystyrene material at 120 ^{o}C [42].

Term	E_{PS}	Relaxation Time τ_i (s)
1	6.72×10^{-06}	0.04125
2	0.18888	0.04639
3	0.52196	1.04173
4	0.28914	35.23156

Table 4
Prony series coefficients to obtain the modulus relaxation of polystyrene material at 140 ^{o}C.

Term	E_{PS}	Relaxation Time τ_i (s)
1	0.72989	0.38354
2	0.09987	2.71861
3	0.17024	12.23223

Data availability

Data will be made available on request.

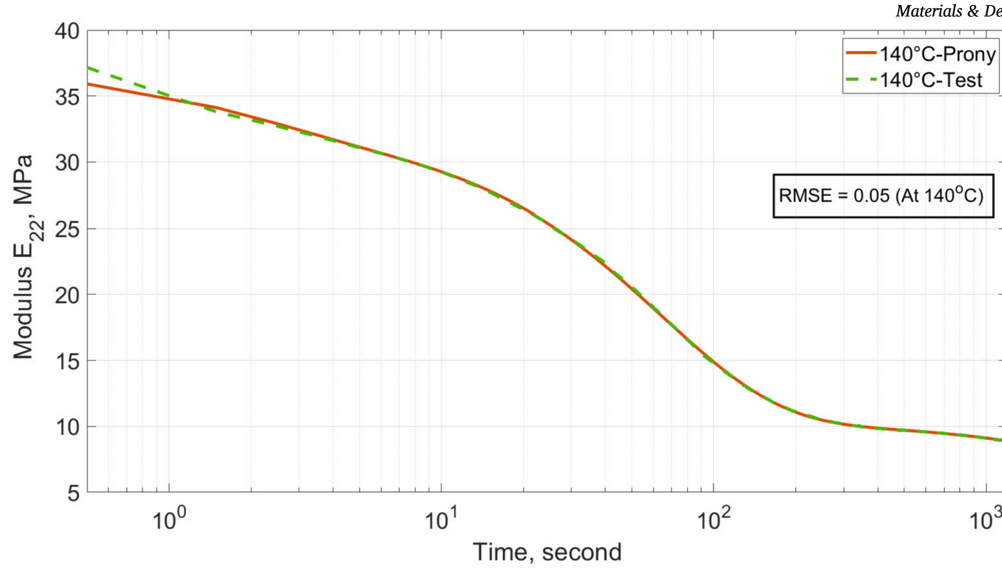

Fig. 16. The transverse modulus E_{22} relaxation at 140 ^{o}C for 20 minutes (SkyFlex K51).

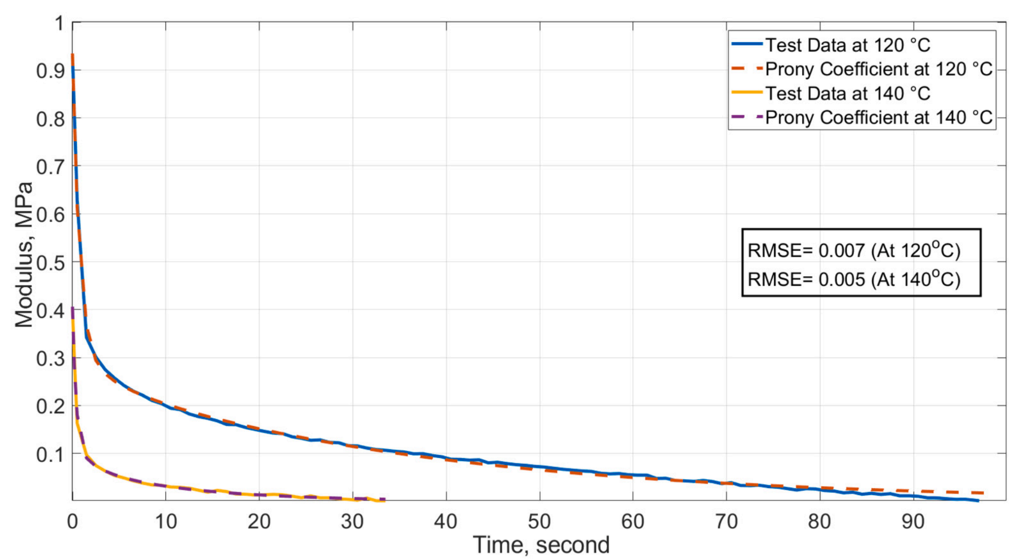

Fig. 17. Modulus relaxation at 120 ^{o}C and 140 ^{o}C (Polystyrene PS material).

References

[1] T.-W. Liu, J.-B. Bai, N. Fantuzzi, H.-T. Xi, H. Xu, S.-L. Li, P.-C. Cao, Folding behavior of thin-walled tubular deployable composite boom for space applications: experiments and numerical simulation, Acta Astronaut. 209 (2023) 159–171.

[2] G. De Zanet, A. Viquerat, G. Aglietti, Predicted thermal response of a deployable high-strain composite telescope in low-earth orbit, Acta Astronaut. 205 (2023) 127–143.

[3] A. Tresoldi, J. Shore, A.C. Austin, G.S. Aglietti, Development of a deployable synthetic aperture radar antenna for a nanosatellite conceptual design, Acta Astronaut. 210 (2023) 488–497.

[4] J.-B. Bai, D. Chen, J.-J. Xiong, R.A. Shenoi, Folding analysis for thin-walled deployable composite boom, Acta Astronaut. 159 (2019) 622–636.

[5] T.-W. Liu, J.-B. Bai, Z.-Z. Wang, N. Fantuzzi, Determining folded stable state of bistable deployable composite boom: an improved two-parameter analytical model, Acta Astronaut. 213 (2023) 507–515.

[6] M.J. Silver, M.A. Echter, B.M. Reid, J. Banik, Precision high strain composite hinges for the deployable in-space coherent imaging telescope, in: 3rd AIAA Spacecraft Structures Conference, 2016, p. 0969.

[7] M.A. Echter, M.J. Silver, E. D'Elia, M. Peterson, B.M. Reid, Recent developments in precision high strain composite hinges for deployable space telescopes, in: 2018 AIAA Spacecraft Structures Conference, 2018, p. 0939.

[8] L. Blanchard, G. Aridon, F. Falzon, D. Remond, R. Dufour, A tape-spring hexapod for deployable telescopes: dynamics, in: International Conference on Space Optics—ICSO 2006, vol. 10567, International Society for Optics and Photonics, 2017, p. 1056718.

[9] G. Aridon, L. Blanchard, D. Remond, R. Dufour, Modal identification for modeling a deployed tape-spring hexapod, in: 47th AIAA/ASME/ASCE/AHS/ASC Structures, Structural Dynamics, and Materials Conference 14th AIAA/ASME/AHS Adaptive Structures Conference 7th, 2006, p. 1977.

[10] O. Soykasap, S. Pellegrino, P. Howard, M. Notter, Folding large antenna tape spring, J. Spacecr. Rockets 45 (3) (2008) 560–567.

[11] J. Yee, S. Pellegrino, Folding of woven composite structures, Composites, Part A, Appl. Sci. Manuf. 36 (2) (2005) 273–278.

[12] T.W. Murphey, W. Francis, B. Davis, J.M. Mejia-Ariza, High strain composites, in: 2nd AIAA Spacecraft Structures Conference, 2015, p. 0942.

[13] K. Seffen, S. Pellegrino, Deployment of a Rigid Panel by Tape-Springs, Cambridge University Department of Engineering, 1997.

[14] H. Mallikarachchi, Thin-walled composite deployable booms with tape-spring hinges, Ph.D. thesis, University of Cambridge, 2011.

[15] R. Guo, X. Jin, Q. Jia, X. Ma, N. An, J. Zhou, Folding, stowage, and deployment of composite thin-walled lenticular tubes, Acta Astronaut. 213 (2023) 567–577.

[16] F. Beavers, N. Munshi, M. Lake, A. Maji, K. Qassim, B. Carpenter, S. Rawal, Design and testing of an elastic memory composite deployment hinge for spacecraft, in: 43rd AIAA/ASME/ASCE/AHS/ASC Structures, Structural Dynamics, and Materials Conference, 2002, p. 1452.

[17] J.W. Jeong, Y.I. Yoo, D.K. Shin, J.H. Lim, K.W. Kim, J.J. Lee, A novel tape spring hinge mechanism for quasi-static deployment of a satellite deployable using shape memory alloy, Rev. Sci. Instrum. 85 (2) (2014) 025001.

[18] D. Margoy, I. Gouzman, E. Grossman, A. Bolker, N. Eliaz, R. Verker, Epoxy-based shape memory composite for space applications, Acta Astronaut. 178 (2021) 908–919.
[19] T.D. Dao, N.S. Ha, N.S. Goo, W.-R. Yu, Design, fabrication, and bending test of shape memory polymer composite hinges for space deployable structures, J. Intell. Mater. Syst. Struct. 29 (8) (2018) 1560–1574.
[20] W. Francis, M. Lake, K. Mallick, G. Freebury, A. Maji, Development and testing of a hinge/actuator incorporating elastic memory composites, in: 44th AIAA Structures, Structural Dynamics, and Materials Conference, Norfolk, VA, April 2003, pp. 7–10.
[21] M.S. Lake, D. Campbell, The fundamentals of designing deployable structures with elastic memory composites, in: 2004 IEEE Aerospace Conference Proceedings (IEEE Cat. No. 04TH8720), vol. 4, IEEE, 2004, pp. 2745–2756.
[22] X. Lan, Y. Liu, H. Lv, X. Wang, J. Leng, S. Du, Fiber reinforced shape-memory polymer composite and its application in a deployable hinge, Smart Mater. Struct. 18 (2) (2009) 024002.
[23] T. Liu, L. Liu, M. Yu, Q. Li, C. Zeng, X. Lan, Y. Liu, J. Leng, Integrative hinge based on shape memory polymer composites: material, design, properties and application, Compos. Struct. 206 (2018) 164–176.
[24] S.C. Arzberger, M.L. Tupper, M.S. Lake, R. Barrett, K. Mallick, C. Hazelton, W. Francis, P.N. Keller, D. Campbell, S. Feucht, et al., Elastic memory composites (emc) for deployable industrial and commercial applications, in: Smart Structures and Materials 2005: Industrial and Commercial Applications of Smart Structures Technologies, vol. 5762, International Society for Optics and Photonics, 2005, pp. 35–48.
[25] G. Ming, L. Liu, Y. Liu, J. Leng, Space deployable parabolic reflector based on shape memory polymer composites, Compos. Struct. 304 (2023) 116327.
[26] X. Lan, L. Liu, Y. Liu, J. Leng, S. Du, Post microbuckling mechanics of fibre-reinforced shape-memory polymers undergoing flexure deformation, Mech. Mater. 72 (2014) 46–60.
[27] M.S. Lake, D. Campbell, The fundamentals of designing deployable structures with elastic memory composites, in: 2004 IEEE Aerospace Conference Proceedings (IEEE Cat. No. 04TH8720), vol. 4, IEEE, 2004, pp. 2745–2756.
[28] E. Abrahamson, M. Lake, N. Munshi, K. Gall, Shape memory polymers for elastic memory composites, in: 43rd AIAA/ASME/ASCE/AHS/ASC Structures, Structural Dynamics, and Materials Conference, 2002, p. 1562.
[29] S.C. Arzberger, M.L. Tupper, M.S. Lake, R. Barrett, K. Mallick, C. Hazelton, W. Francis, P.N. Keller, D. Campbell, S. Feucht, et al., Elastic memory composites (emc) for deployable industrial and commercial applications, in: Smart Structures and Materials 2005: Industrial and Commercial Applications of Smart Structures Technologies, vol. 5762, International Society for Optics and Photonics, 2005, pp. 35–48.
[30] F. Lopez Jimenez, Mechanics of thin carbon fiber composites with a silicone matrix, Ph.D. thesis, California Institute of Technology, 2011.
[31] C. Wang, Y. Wang, The mechanical design of a hybrid intelligent hinge with shape memory polymer and spring sheet, Composites, Part B, Eng. 134 (2018) 1–8.
[32] J.H. Lim, Y.-B. Kim, I.-S. Jang, H. Kim, H.-U. Oh, Parabolic deployable mesh antenna with a hingeless system of superelastic sma ribs and composite tape springs, Acta Astronaut. 200 (2022) 149–162.
[33] O. Testoni, T. Lumpe, J.-L. Huang, M. Wagner, S. Bodkhe, Z. Zhakypov, R. Spolenak, J. Paik, P. Ermanni, L. Muñoz, et al., A 4d printed active compliant hinge for potential space applications using shape memory alloys and polymers, Smart Mater. Struct. 30 (8) (2021) 085004.
[34] T. Saito, T. Kuwahara, A. Pala, Y. Miyazaki, T. Kaneko, Fem dynamic simulation technique for membrane structure deployment and model evaluation, Acta Astronaut. 218 (2024) 342–355.
[35] J. Hao, A. Ning, J. Qilong, S. Chun, M. Xiaofei, Z. Jinxiong, Multi-objective topology optimization for cutout design in deployable composite thin-walled structures, Chin. J. Aeronaut. (2025) 103530.
[36] Z. Soltani, M. Santer, Refined unified formulation for efficient folding and unfolding analyses of slender thin-walled structures, AIAA J. 60 (9) (2022) 5559–5569.
[37] P. Kunakorn-ong, Z. Soltani, M. Santer, Optimal design of tube flexure cut-out geometries for deployment performance, Acta Astronaut. 197 (2022) 35–45.
[38] A. Ahmed, I.U. Din, S. Kulkarni, K.A. Khan, Multiscale finite element modeling of origami-inspired dual matrix deployable composite with visco-hyperelastic hinge, Compos. Struct. 343 (2024) 118301.
[39] I.U. Din, A. Ahmed, F. Tarek, W. Cantwell, K.A. Khan, Ultra-thin composites membrane for deployable structures: Xct driven characterization and fe modeling of folding structure, Compos. Sci. Technol. 245 (2024) 110341.
[40] I.U. Din, A. Ahmed, K.A. Khan, Origami-inspired self-sensing foldable composite structures: experiments and modeling, Comp. Part C Open Access 17 (2025) 100583.
[41] P. Robinson, A. Bismarck, B. Zhang, H.A. Maples, Deployable, shape memory carbon fibre composites without shape memory constituents, Compos. Sci. Technol. 145 (2017) 96–104.
[42] M. Almuslmani, M.J. Santer, Tape-spring hinges with controllable stiffness composite materials, in: AIAA SCITECH 2024 Forum, 2024, p. 1044.
[43] F. Gandhi, S.-G. Kang, Beams with controllable flexural stiffness, Smart Mater. Struct. 16 (4) (2007) 1179.
[44] G. Murray, F. Gandhi, S.-G. Kang, Flexural stiffness control of multilayered beams, AIAA J. 47 (3) (2009) 757–766.
[45] H.A. Maples, P. Robinson, A. Bismarck, High performance carbon fibre reinforced polymer composites with controllable stiffness: can it be done, in: ECCM15, 2012.
[46] H.A. Maples, S. Wakefield, P. Robinson, A. Bismarck, High performance carbon fibre reinforced epoxy composites with controllable stiffness, Compos. Sci. Technol. 105 (2014) 134–143.
[47] B. Zhang, P. Robinson, A. Bismarck, H. Maples, C. Burgstaller, An investigation of the viscoelastic behaviour of interleaved composite with shape memory capability, in: 21st International Conference on Composite Materials, 2017.
[48] H. Maples, P. Robinson, B. Zhang, A. Bismarck, W. Li, C. Burgstaller, Exploring Deployable Configurations Using Interleaved Composite with Shape Memory Capability, 2017.
[49] G.G. Murali, High-performance shape memory composites with intrinsic heating capabilities, Ph.D. thesis, Imperial College London, 2023.
[50] H.A. Maples, O. Smith, C. Burgstaller, P. Robinson, A. Bismarck, Improving the ply/interleaf interface in carbon fibre reinforced composites with variable stiffness, Compos. Sci. Technol. 128 (2016) 185–192.
[51] B. Zhang, Interleaved composites for controllable stiffness, shape memory and easy repair capabilities, Ph.D. thesis, Imperial College London, 2020.
[52] N.G. McCrum, C.P. Buckley, C.B. Bucknall, Principles of Polymer Engineering, Oxford University Press, 1997.
[53] R.J. Young, P.A. Lovell, Introduction to Polymers, CRC Press, 2011.
[54] H.F. Brinson, L.C. Brinson, et al., Polymer engineering science and viscoelasticity, An introduction 99 (2008) 157.
[55] M.J. Santer, Composite tube flexures at nanosatellite scale, in: 4th AIAA Spacecraft Structures Conference, 2017, p. 0622.
[56] S.K. Chemicals, Skyflex materials selection guide (version 2.0), Tech. Rep., SK Chemicals, technical Data Sheet, 2015, https://www.skchemicals.com/download/TDS/SKYFLEX/SKYFLEX_MSG_ver2.0.pdf.
[57] INEOS Styrolution, Styrolution ps 124n/l – general purpose polystyrene (gpps), Tech. Rep., INEOS Styrolution, technical Data Sheet, 2016, https://www.ineos-styrolution.com/Product/GPPS_Styrolution-PS-124N-L_SKU200300060569.html.
[58] H. Maples, Composites with controllable stiffness, Ph.D. thesis, Imperial College London, 2014.
[59] P. Kunakorn-ong, M. Santer, Optimal design of tube flexure cut-out geometries for viscoelastic resilience and deployment performance, Acta Astronaut. 216 (2024) 282–294.